Title

First Cerenkov charge-induction (CCI) TlBr detector for TOF-PET and proton range verification

Journal

Physics in Medicine and Biology, 64(17)

ISSN

0031-9155

Authors

Ariño-Estrada, Gerard
Mitchell, Gregory S
Kim, Hadong
et al.

Publication Date

2019-09-01

DOI

10.1088/1361-6560/ab35c4

Peer reviewed

HHS Public Access

Author manuscript

Phys Med Biol. Author manuscript; available in PMC 2021 June 09.

Published in final edited form as:

Phys Med Biol. ; 64(17): 175001. doi:10.1088/1361-6560/ab35c4.

First Cerenkov Charge-Induction (CCI) TlBr Detector for TOF-PET and Proton Range Verification

Gerard Ariño-Estrada[1], **Gregory S Mitchell**[1], **Hadong Kim**[2], **Junwei Du**[1], **Sun Il Kwon**[1], **Leonard J Cirignano**[2], **Kanai S Shah**[2], **Simon R Cherry**[1]

[1]Department of Biomedical Engineering, University of California Davis, Davis, CA

[2]Radiation Monitoring Devices, Inc., Watertown, MA

Abstract

Thallium bromide (TlBr) is a semiconductor material and, simultaneously, a good Cerenkov radiator. The performance of a TlBr detector that integrates two different readouts, the charge induction readout and the detection of Cerenkov light, was evaluated. A TlBr detector with dimensions of 4×4×5 mm^3, with a monolithic cathode and an anode segmented into strips, was manufactured. One of the bare and polished 4×4 mm^2 faces of the detector was coupled to a silicon photomultiplier (SiPM) to read out the Cerenkov light. Simultaneous timing and energy resolutions of <400 ps full width at half maximum (FWHM) and ~8.5% at 511 keV, were measured using the Cerenkov detection and charge induction readouts, respectively. A coincidence time resolution of 330 ps was obtained when selecting Cerenkov events with amplitudes above 70 mV. The combination of both readouts showed the potential to resolve the depth-of-interaction (DOI) positioning, based on the improvement of energy resolution when selecting events with similar electron drift times. This manuscript sets the stage for a new family of semiconductor detectors that combine charge induction readout with the Cerenkov light detection. Such detectors can provide, simultaneously, outstanding timing, energy, and spatial resolution, and will be an excellent fit for applications that require the detection of high-energy gamma photons with high timing accuracy, such as time-of-flight positron emission tomography (TOF-PET) and prompt gamma imaging (PGI) to assess the particle range in hadron therapy.

Introduction

Semiconductor radiation detectors are an attractive choice for applications that require good energy resolution and spatial localization. Semiconductor materials with high atomic number and density, such as cadmium telluride (CdTe), cadmium zinc telluride (CZT), and thallium bromide (TlBr) provide much higher detection efficiency compared to other commonly used semiconductors such as silicon. High detection efficiency is an indispensable trait for detectors when used in medical imaging applications.

The utilization of CdTe or CZT in full-size positron emission tomography (PET) scanners has been studied (Ishii et al. 2007) and has provided very competitive spatial resolution. However, the timing properties of state-of-the-art time-of-flight PET (TOF-PET) scanners, which have <500 ps timing resolution, are extremely challenging for semiconductor detectors to match. CdTe and CZT detector-based benchtop systems have achieved, at best,

~5–10 ns full width at half maximum (FWHM) coincidence time resolution (CTR) (Abbaszadeh and Levin 2017, Ariño et al. 2013, Groll et al. 2016, Mitchell et al. 2008, Morimoto et al. 2011, Vaska et al. 2007). Furthermore, CdTe and CZT are not competitive in terms of stopping power compared to the dense scintillators commonly used in PET scanners.

Timing resolution in semiconductor detectors is intrinsically limited by the difference of the mobility of electrons and holes (Owens 2016). A dramatic improvement in the timing properties of TlBr was achieved by using the Cerenkov light emitted promptly after the interaction of a gamma ray with the TlBr bulk (Ariño-Estrada et al. 2018a). CTR as good as 430 ps FWHM was measured between a TlBr crystal of dimensions 3×3×5 mm^3 and a reference detector. Two properties in combination uniquely position TlBr to work with this approach: First, the very high index of refraction of 2.6, which lowers the threshold for Cerenkov light generation and therefore increases the Cerenkov light yield. Second, the transparency of TlBr above approximately 460 nm (Ariño-Estrada et al. 2018a) due to its relatively large bandgap energy of 2.6 eV. A similar approach is not practical in CdTe or CZT, as the material is only transparent at long wavelengths where there is very little Cerenkov emission.

The utilization of Cerenkov light as a fast timing signal in TlBr might be combined with the standard charge induction readout of semiconductor detectors in the same device to achieve an outstanding performance, simultaneously, in energy, spatial, and timing resolution, as well as detection efficiency. In fact, TlBr has better stopping power at 511 keV than any of the traditional scintillators used for PET imaging. Such a detector would be of interest for the next generation of TOF-PET detectors and carries the additional advantages over commonly-used lutetium (Lu)-based scintillators of no background, and a material that should be very economic to produce in large quantities because of low raw material costs, low melting temperature, and tendency to form large crystal grains (Hitomi et al. 2011). Further, it could be used for *in vivo* proton range verification (PRV) in hadron therapy, by detecting the highly energetic prompt-gammas emitted near the Bragg peak (Pausch et al. 2018).

In this manuscript, the first-ever semiconductor detector that simultaneously combines the detection of Cerenkov light with the signals induced in the electrodes by the charge carriers is presented. This new kind of detector is called a Cerenkov Charge Induction (CCI) TlBr detector. The timing resolution of this detector, based on the Cerenkov light detection, the energy performance, based on the charge induction readout, and the depth of interaction (DOI) estimation by combining both readouts, are reported. This work will set the stage for a new family of detectors able to provide high performance in time, energy, and spatial resolution, as well as high detection efficiency for gamma photons.

Materials and Methods

The TlBr was grown by the traveling molten zone (TMZ) method, more details on the material growth can be found in Churilov et al. (2008). A parallelepiped, slightly larger than 4mm × 4mm × 5mm, was cut from a TlBr wafer. This sample was then lapped, polished and

chemically etched. An electrode layer was deposited on two opposed 4×5 mm^2 faces. One of the electrodes was segmented into strips of 0.4 mm width and 0.1 mm inter-strip distance. The detector was mounted on a custom printed circuit board (PCB) and the 4×5 mm^2 faces were wrapped with Teflon tape to act as a reflector. The top 4×4 mm^2 face of the detector was placed in direct contact with a silicon photomultiplier (SiPM) S14160-3050HS (Hamamatsu Photonics K.K., Hamamatsu, Japan) using a small volume of optical grease (BC-630, Saint-Gobain, Courbevoie, France). Figures 1a–c shows several photographs of the detector. The optical readout of the CCI TlBr detector will be referred to as "TlBr-SiPM" in the rest of the manuscript.

The CCI TlBr detector was operated in coincidence with a reference detector to evaluate its timing properties, the setup is depicted in Fig. 1-d. A ^{22}Na source with an approximate activity of 4.44 MBq (120 μCi) was used. The reference detector consisted of a lutetium fine silicate (LFS) scintillation crystal with dimensions 3×3×20 mm^3 coupled to a S14160-3050HS (Hamamatsu Photonics K.K.) SiPM. Both SiPMs were operated at 20°C and a biased at 40.5 V, 3.5 V over-voltage.

The SiPMs were read out using the Ketek Eval-Kit PCB (Ketek GmbH, Münich, Germany). The output signals were digitized using the DRS4 evaluation board from Paul Scherrer Institute (PSI, Villigen, Switzerland), with a sampling rate of 5 Gs/s and a record length of, approximately, 200 ns. The DRS4 was set to trigger on coincidences between the preamplifier signals of both SiPMs, with a trigger threshold of 450 mV and 5 mV in the reference and TlBr-SiPM detector, respectively. Three waveforms were recorded per event: the preamplifier output of the reference detector, the raw output of the reference detector, and the preamplifier output of the TlBr-SiPM.

The digitized preamplifier output signals of each SiPM were analyzed to obtain the detection time. Leading edge thresholding was used, with the trigger threshold set at 3.5 mV following subtraction of the baseline of each signal. Linear interpolation between the two closest points to the amplitude threshold was used to obtain the time stamp. The amplitude of the monitor signal of the reference detector was used to measure the energy deposited in the reference detector. The monitor signal of the TlBr-SiPM was not recorded as it was too weak to provide any meaningful information.

The readout board described in Ariño-Estrada *et al* (2018b) was used to measure the energy resolution. Seven anode strips of the CCI detector were each connected to a charge sensitive preamplifier CR110 (Cremat, West Newton, MA) to keep them at the same potential. The bias voltage was applied to the common electrode and its signal was not read out. The preamp output of a representative strip located in the center of the detector was read out and will be referred to as "charge induction signal" in this manuscript. The charge induction signal was split. One branch was fed into a spectroscopy amplifier (Canberra model 2021 (currently part of Mirion Technologies, Inc.), San Ramon, CA), with a shaping time of 10 μs, and was used to measure the energy. The other branch was fed into a fast filter amplifier (FFA) 579 (ORTEC, Oak Ridge, TN) with integration and differentiation times of 500 ns. This branch was used to measure the drift time of electrons.

The outputs of the spectroscopy amplifier and the FFA were digitized with a desktop digitizer DT5740D (CAEN Inc., Via Reggio, Italy) with a sampling rate of 62.5 Ms/s and a record length of approximately 64 μs. The trigger output of the DRS4 board was used as an external trigger for the DT5740D. The trigger time in the DT5740D was set at 40% of the record length, thus acquiring for 25.6 μs prior to the trigger, and for 38.4 μs after the trigger. The baseline of the spectroscopy amplifier signal was subtracted and its maximum amplitude and was used as the energy measurement of the event. The trigger signal was in a common position for all the events and was used as the start signal for the electron drift, while the peak of the FFA signal was used as the stop. The difference between these two points was taken as the measurement of the electron drift time. The detector was biased at −800 V and kept at 20°C.

Results

Figure 2-a shows the FWHM of the CTR, as the threshold on the TlBr-SiPM pulse amplitude is varied. The FWHM was evaluated by linear interpolation of the histogram bins immediately above and below the half maximum of the peak on each side of the curve. Uncertainty for each FWHM measurement was taken as the square root of the sum of the square of the distances between each interpolated time point to the furthest adjacent bin. The increase of the uncertainty values with increasing threshold is due to the reduction of counting statistics.

Figure 2-b shows the pulse amplitude distribution for events in the TlBr-SiPM detector. The even distribution of the peaks suggests each peak of greater amplitude corresponds to an increment of one photon. However, a comprehensive characterization of the SiPM noise properties will be needed to confirm these measurements. Figure 2-c shows the coincidence time distribution for all the events in the dataset and a CTR of (370±5) ps. The best result achieved is when events with an amplitude above 70 mV are accepted, yielding a CTR of (330±10) ps FWHM, see Fig. 2-d.

Figure 3-a shows the spectroscopy for all events in the dataset. The majority of events had drift times compressed between 0 and, approximately, 8 μs. The expected maximum electron drift time was ~7 μs. Events with negative or greater drift times were likely due to interactions that took place elsewhere than in the active volume defined by the strip and thus provided a random drift time measurement. The 511 keV photopeak and K-edge escape peak (~425 keV) can hardly be resolved due to the high ballistic deficit in the detector.

Figure 3-b shows the spectroscopy of the subset of events with drift times between 4 μs and 4.4 μs. The two energy peaks can be resolved much better in this case and thus shows the potential of significantly improving energy resolution by using the electron drift time measurement. The energy resolution was measured by linear interpolation between the histogram bins above and below the half maximum on each side of the peak and was, approximately 8.5% at 511 keV, which shows potential for improvement by using a depth-correction strategy.

Discussion

Results show that both readouts, Cerenkov light and charge induction, can be utilized simultaneously. Cerenkov events generated by 511 keV gammas show a CTR <400 ps FWHM, which allows CCI TlBr detectors to be used in TOF-PET. Moreover, for the subset of events with greater amplitudes, the CTR improves to 330 ps FWHM. The very significant improvement of energy resolution based on the drift time gating shows the potential for energy measurement correction based on the drift time. Prompt gamma timing (Golnik et al. 2014) is a very good fit to CCI detectors as well given its timing resolution and the much higher yield of generation of Cerenkov photons for gammas >1 MeV of energy. The energy resolution could be used in PRV for prompt gamma spectroscopy (Hueso-González et al. 2018) in combination with the PGT to improve the range assessment accuracy.

CCI TlBr detectors can provide 3-D spatial localization by combining electrode segmentation and DOI estimation. An individual drift time-energy measurement calibration per device would account for the typical variability of drift properties of charge carriers in compound semiconductor materials (Ariño-Estrada *et al* 2014). Next steps in the development of CCI TlBr detectors will include the study of variability among different anode elements in the same device, a thorough characterization of their positioning capabilities, variability of electron drift times among devices extracted from the same ingot, and effects between anode elements such as charge sharing. The potential fine 3-D segmentation and high energy resolution of CCI TlBr detectors make them very good candidates to build Compton telescopes for high energy gammas (Llosá et al. 2016, Draeger et al. 2018). A very accurate analysis of the Cerenkov radiation created by the detection of high energy gammas might allow estimation of the momentum of the Compton recoil electron to reduce the uncertainty of the measurement of the Compton angle.

Different CCI detector configurations from the one presented in this work might be studied in the near future. Dual-sided-strip-detector readout or a pixelated anode with a monolithic cathode can be pursued. The combination of position-sensitive virtual Frisch grid readout (Bolotnikov et al. 2016) and Cerenkov light detection could provide extremely high energy and spatial resolution as well. All these options would provide the outstanding timing accuracy, 3-D positioning, and energy resolution that characterize CCI detectors.

Besides providing outstanding timing accuracy, the Cerenkov readout might help with resolving pile-up events or providing information about the recoil electron in Compton interactions between gammas and the TlBr. CCI detectors are a novel and promising choice for the detection of high energy gamma rays for applications that require very good timing, spectroscopic, and spatial resolution.

Acknowledgments

This work was supported by NIH grants R01 CA183994, R35 CA197608 and R03 EB025533, and a UC Davis Academic Federation Innovative Developmental Award. The authors would like to thank Dr. Armin Kolb, and Aaron Selfridge for helpful discussions, and Hamamatsu Photonics K.K. for graciously providing the SiPM samples.

References

Abbaszadeh S and Levin CS, “New-generation small animal positron emission tomography system for molecular imaging”, J. Med. Imaging, 4(1):011008 (2017).

Ariño G et al., “Energy and coincidence time resolution measurements of CdTe detectors for PET”, J. Instrum, C02015 (2013). [PubMed: 23750177]

Ariño-Estrada G, Chmeissani M, de Lorenzo G, Kolstein M, Puigdengoles C, Garcia C, Cabruja E, “Measurement of mobility and lifetime of electrons and holes in a Schottky CdTe diode” J. Instrum C12032 (2014). [PubMed: 25729405]

Ariño-Estrada G, Mitchell GS, Kwon SI, Du J, Kim H, Cirignano LJ, Shah KS, Cherry SR., “Towards Time of Flight PET with a Semiconductor Detector”, Phys. Med. Biol, 63 04LT01 (2018a).

Ariño-Estrada G, Du J, Kim H, Cirignano LJ, Shah KS, Cherry SR, Mitchell GS, “Development TlBr Detectors for PET Imaging”, Phys. Med. Biol, 63 13NT01 (2018b).

Bolotnikov AE, et al., “CdZnTe position-sensitive drift detectors with thicknesses up to 5 cm”, Appl. Phys. Lett, 108, 093504 (2016).

Churilov AV, Higgins WM, Ciampi G, Kim H, Cirignano LJ, Olschner F, Shah KS, “Purification, crystal growth and detector performance of TlBr”, Proc. SPIE 7079, Hard X-Ray, Gamma-Ray, and Neutron Detector Physics X, 70790K (2008).

Draeger E, Mackin D, Peterson S, Chen H, Avery S, Beddar S, Polf JC, “3D prompt gamma imaging for proton beam range verification”, Phys. Med. Biol, 63:035019 (2018). [PubMed: 29380750]

Golnik C, et al., “Range assessment in particle therapy based on prompt γ-ray timing measurements”, Phys. Med. Biol, 59:5399–5422 (2014). [PubMed: 25157685]

Groll A, Kim K, Bhatia H, Zhang JC, Wang JH, Shen ZM, Cai L, Dutta J, Li Q, Meng LJ, “Hybrid pixel-waveform (HPWF) enabled CdTe detectors for small animal gamma-ray imaging applications”, IEEE Tran. Rad. Plas. Med. Sci, 1(1):3–14 (2016).

Hitomi K, Tada T, Kim S-Y, Wu Y, Tanaka T, Shoji T, Yamazaki H, Ishii K, “Recent Development of TlBr Gamma-Ray Detectors”, IEEE Trans. Nucl. Sci, 58(4):1987–1991 (2011).

Hueso-González F, Rabe M, Ruggieri TA, Bortfeld T, Verburg JM, “A full scale clinical prototype for proton range verification using prompt gamma-ray spectroscopy”, Phys. Med. Biol, 63:185019 (2018). [PubMed: 30033938]

Ishii K, et al., “First achievement of less than 1 mm FWHM resolution in practical semiconductor animal PET scanner”, Nucl. Instum. Meth. A, 576(2–3):435–440 (2007).

Llosá G, et al., “First Images of a Three-Layer Compton Telescope Prototype for Treatment Monitoring in Hadron Therapy”, Front. Oncol, 6:14 (2016). [PubMed: 26870693]

Mitchell GS, Sinha S, Stickel JR, Bowen SL, Cirignano LJ, Dokhale P, Kim H, Shah KS, Cherry SR, “CdTe strip detector characterization for high resolution small animal PET”, IEEE Tran. Nuc. Sci 55(3):870–876 (2008).

Morimoto Y, et al. “Development of a 3D Brain PET Scanner Using CdTe Semiconductor Detectors and Its First Clinical Application”. IEEE Trans. Nucl. Sci 58(5): 2181–2189 (2011).

Owens A, “Compound semiconductor radiation detectors”, CRC Press, Boca Raton, FL, USA (2016).

Pausch G, Berthold J, Enghardt W, Römer K, Straessner A, Wagner A, Werner T, Kögler T, “Detection systems for range monitoring in proton therapy: Needs and challenges”, Nucl. Instrum. Meth, A in press (2018).

Vaska P, et al., “A Prototype CZT-based PET Scanner for High Resolution Mouse Brain Imaging” IEEE Nucl. Sci. Symp. Conf. Rec., M19–171 (2007).

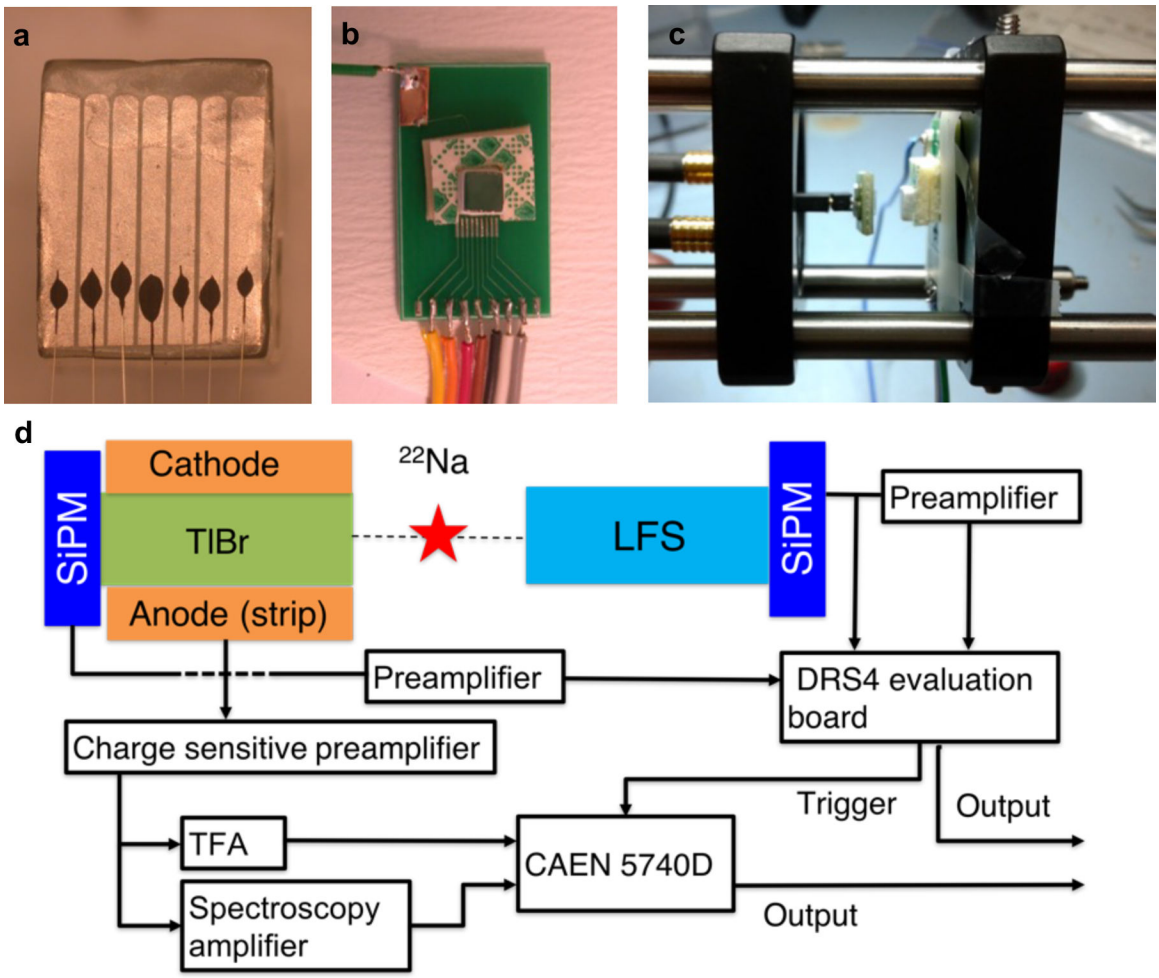

Figure 1.

a) Segmented electrode of the CCI detector used in the measurements. b) Hybrid TlBr detector mounted on a custom PCB board. c) mechanism used to couple the SiPM to a CCI TlBr detector d) Schematic of the readout setup.

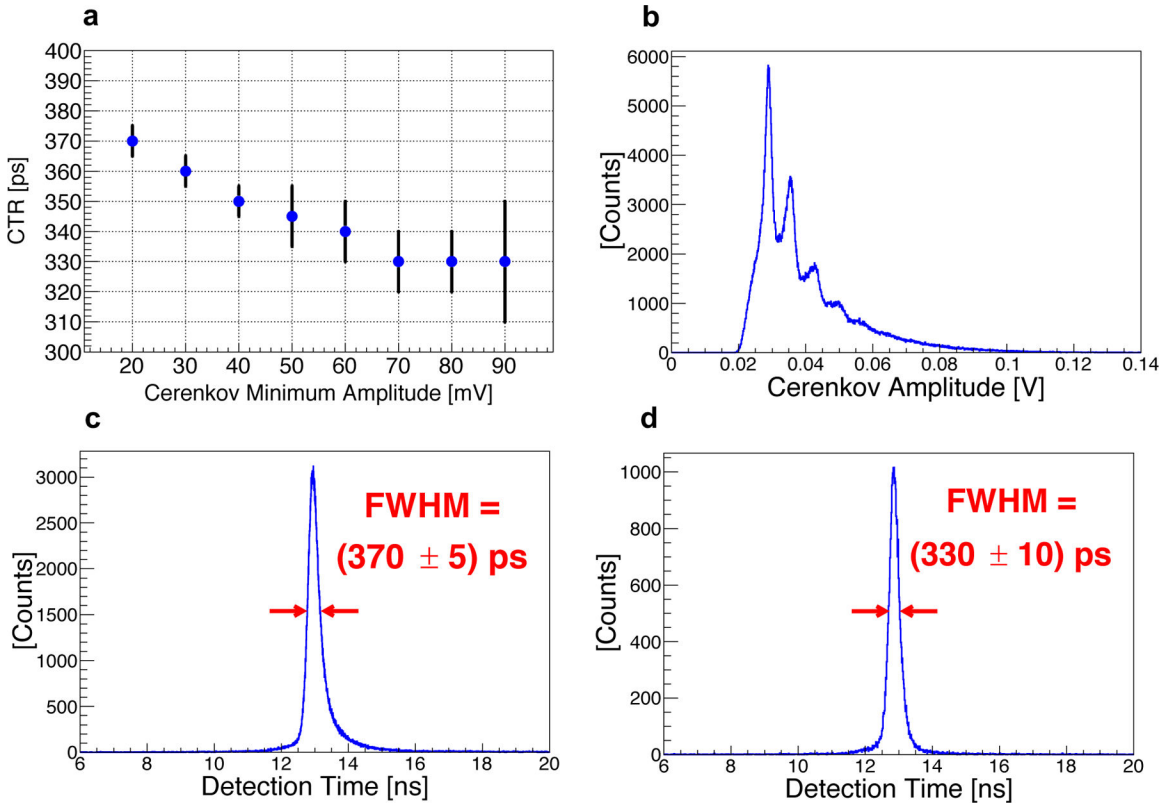

Figure 2.

All plots were obtained from the same dataset. Coincidence events with deposited energy in the reference detector around the 511 keV peak were included. a) CTR vs minimum amplitude acceptance of events in the TlBr-SiPM detector. Error bars are derived from the linear interpolation used to obtain the FWHM. b) Pulse amplitude of the TlBr-SiPM readout, referred to as Cerenkov amplitude. c) CTR for events with an amplitude in the TlBr-SiPM detectors above 20 mV. d) CTR for events with an amplitude in the TlBr-SiPM detectors above 70 mV.

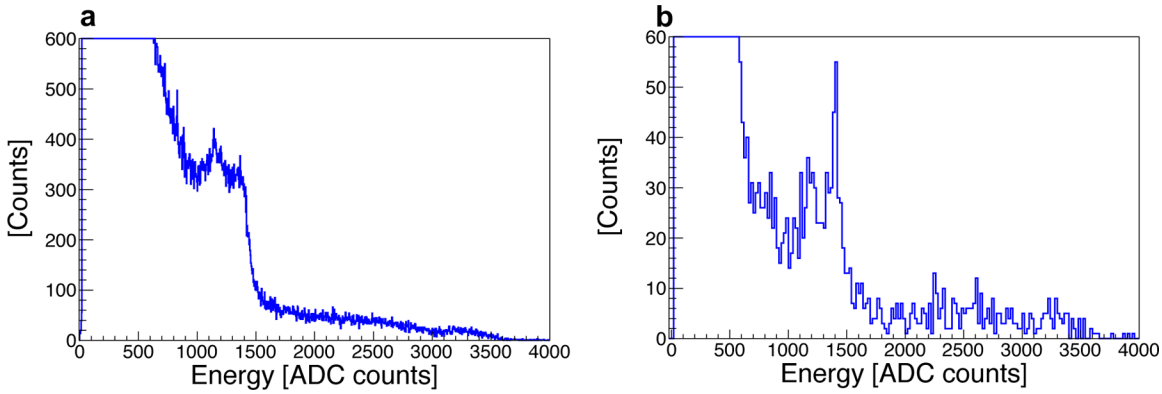

Figure 3.

All plots come from the same dataset shown in Fig. 2. Coincidence events with any deposited energy in the reference detector were included. a) Spectroscopy of the ^{22}Na source using the charge induction readout. b) ^{22}Na spectroscopy of the subset of (a) with events with selected electron drift times between 4 μs and 4.4 μs. Energy resolution at the 511 keV photopeak is ~8.5%.